RSC Advances

PAPER

View Article Online
View Journal | View Issue

Cite this: *RSC Adv.*, 2020, **10**, 5050

Self-healing composite hydrogel with antibacterial and reversible restorability conductive properties†

Mimpin Ginting, ‡*[a] Subur P. Pasaribu, ‡[b] Indra Masmur,[a] Jamaran Kaban[a] and Hestina[c]

Received 4th January 2020
Accepted 24th January 2020

DOI: 10.1039/d0ra00089b

rsc.li/rsc-advances

Self-healable PAA/PPy–Fe composite hydrogels have been simply synthesized in one step and utilized for antibacterial and electrical conductivity application. The network of hydrogel is composed of polyacrylic acid (PAA) and Fe^{3+} ions with interlacing of the second polymeric chain of polypyrrole (PPy). In this study, ammonium persulfate (APS) was utilized to initiate the polymerization of both acrylic acid and pyrrole. Such hydrogels exhibited good mechanical properties and remarkable self-healing efficiency as well. The self-healing ability of the hydrogels was facilitated by ionic interaction between carboxylic anion groups (COO–) from polyacrylic acid (PAA) and Fe^{3+} ions. Moreover, the antibacterial activity of the composite hydrogels was examined on *Escherichia coli via* the disk diffusion method and the zone of inhibition was obtained in the range of 1.26–1.56 cm after incubation for 12 h. In addition, demonstration of the PAA/PPy–Fe composite hydrogels in electrical conductivity applications was performed in which the composite hydrogel was set up in an electrical circuit consisting of an LED and powered by 3 V batteries. The results showed that the electricity could light-up the LED through the PAA/PPy–Fe composite hydrogels and possessed reversible restorability, as indicated by the healed hydrogel consistently lighting-up the LED in the electrical circuit.

Introduction

Self-healing hydrogels are 3D cross-linked hydrophilic polymer networks and able to repair or restore to the original functionalities automatically after being damaged without any external stimuli. Hydrogels provide superior properties such as retain considerable amounts of water, biocompatibility, biodegradable, and elasticity.[1–3] Owing to such properties, hydrogels have attracted considerable attention and are widely used in drug delivery, wound healing, bio-inspired materials, biosensors and many other applications.[4–7] On the other hand, there are remaining challenges; in particular, the lifespan and durability of hydrogels, such as their poor mechanical properties.[8] Acrylic acid is the monomer of poly(acrylic) acid (PAA) which contains unsaturated carboxylic acid groups and tends to be hydrophilic, exhibit good absorption ability and be responsive to pH. Due to the ionic character of the carboxylic groups (–COOH), PAA can be cross-linked with multivalent ions. For instance, Wei *et al.* (2013) synthesized a self-healing hydrogel induced by the migration of ferric ions (Fe^{3+}) which was applied as a protective coating where the hydrogel can protect the glass against mechanical damage.[2] Meanwhile, the self-healing hydrogel of amorphous calcium carbonate ($CaCO_3$)–polyacrylic acid has been fabricated to substitute the conventional plastics.[7] Recently, Pan *et al.* (2019) reported the preparation of triple-physical crosslinking (coordination, hydrogen and electrostatic interactions) self-healing hydrogel by utilizing PAA, aluminium ions (Al^{3+}), and carboxymethyl chitosan nanoparticles which possesses antibacterial properties.[9] However, the reported self-healing hydrogels do not possess conductive properties which might be interesting. Furthermore, hydrogels are usually vulnerable to microorganisms during applications, leading possible infection which is a serious issue. To address this problem, various hydrogels with antimicrobial properties involved multi-steps syntheses were reported.[10,11]

For the last few decades, conductive polymers, such as polyaniline (PANi), polythiophene (PT), polypyrrole (PPy), and poly(3,4-ethylene dioxythiophene) (PEDOT) have drawn researchers' attention due to its electrical properties which are originated from the conjugated π-electron backbone (double bond). The delocalization of electrons is contained in π-bond in which the electrons are free to move over more than two nuclei.[12–14] The conducting polymers were widely used in various application such as biosensors,[15] artificial muscles,[16] drug delivery,[17] and supercapacitors.[18] The resultant conducting

[a]*Department of Chemistry, Faculty of Mathematics and Natural Sciences, Universitas Sumatera Utara, Medan-20155, Indonesia. E-mail: mimpin.ginting@yahoo.com*

[b]*Department of Chemistry, Faculty of Mathematics and Natural Sciences, Mulawarman University, Samarinda-75123, Indonesia*

[c]*Department of Chemistry, Universitas Sari Mutiara Indonesia, Medan-20123, Indonesia*

† Electronic supplementary information (ESI) available. See DOI: 10.1039/d0ra00089b

‡ Ginting M. and Pasaribu S. P. contributed equally to this work.

polymers in most cases are rigid and brittle as a consequence of the delocalized π-electron backbone.

Driven by the challenges of enabling the conductive properties of self-healing hydrogels and to solve the rigidity issue of conducting polymers, herein we reported a simple approach to fabricate PAA/PPy–Fe composite hydrogels with self-healing, antibacterial, and conductive properties. The PAA/PPy–Fe composite hydrogels were synthesized *via* free-radical polymerization. To the best of our knowledge, no study has been reported to synthesize PAA/PPy–Fe composite hydrogels in one-step preparation.

Materials and methods

Materials

Acrylic acid ($CH_2CHCOOH$, 99.1%, Echo Chemical), iron(III) chloride anhydrous ($FeCl_3$, 98%, Sigma-Aldrich), pyrrole (C_4H_5N, 99%, Acros Organics), ammonium persulfate ($(NH_4)_2S_2O_8$, 98%, Sigma-Aldrich), and HCl (37%, Sigma-Aldrich) were analytical grade and used as received without further treatment.

Preparation of PAA/PPy–Fe hydrogels

AA solution with the concentration of 30 w/v% was prepared by dissolving in deionized water, followed by $FeCl_3$ addition of 0.5 mol% of AA with continuous stirring. Afterwards, pyrrole with concentration varied from 5–20 mM were mixed in the solution of AA–$FeCl_3$. The mixture solution was degassed by using N_2 for 30 minutes. Then, the solution was transferred to a Petri dish with an internal diameter of 5 cm and polymerization was performed by adding APS with an amount of 0.15 mol% of AA and conducted at 37 °C for 24 h. On the other hand, the hydrogels without PPy was also synthesized as the control group. Additionally, for the study of Fe^{3+} concentration on hydrogel properties, the concentrations of Fe^{3+} were varied from 0.1 to 0.3, 0.5, 0.7 and 1 mol% of AA while the concentration of pyrrole was fixed at 15 mM. Furthermore, the as-prepared hydrogels were washed by DI water and alcohol for several times to remove unreacted monomers and used for further characterization. For the nomenclature, the obtained hydrogel was named as PAA/PPy_n–Fe where n refers to the concentration of pyrrole (*e.g.* PAA/PPy_{10}–Fe).

FTIR analysis

Samples were analyzed as a powder mixed with KBr powder by Fourier transform infrared method. Spectra were collected in the wavenumber of 4000–400 cm^{-1}, a scan number of 64 and a resolution of 4 cm^{-1} using a Bio-Rad Model FTS-3500GX spectrometer.

Equilibrium degree of swelling (DS) and gel fraction (GF)

Equilibrium swelling degree of the as-prepared hydrogels was determined by gravimetric method. Firstly, the hydrogel samples were immersed in DI water at 37 °C for 48 hours. Subsequently, the swollen hydrogels were wiped gently in order to remove the water excess from the surface and weigh as W_s using an analytical balance. In addition, the effect of pH (1–7) on swelling degree of PAA/PPy–Fe composite hydrogel was also studied. The pH of the swelling solution was adjusted by adding HCl. The equilibrium degree of swelling was calculated by the following equation:

$$\mathrm{DS} = \frac{W_s - W_d}{W_d} \times 100\%$$

From the swelling experiment, the swollen hydrogels were then dried in an oven at 70 °C until a constant weight was obtained and recorded as W_d', the gel fraction was calculated by the following equation:

$$\mathrm{GF} = \frac{W_d'}{W_d} \times 100\%$$

Both swelling and gel fraction experiments were repeated three times and expressed the results as mean ± standard deviation (SD).

Mechanical properties and self-healing efficiency

The composite hydrogels samples were cut into two pieces and allowing the self-healing at 37 °C for 12 h without any external stimulation. Afterwards, the healed hydrogels were subjected to tensile tests (Testometric M500-25AT) with a 100 N load cell and a crosshead speed of 50 mm min^{-1} at room temperature. Finally, the self-healing efficiency of hydrogels is calculated by the following equation:

$$\eta = \frac{\sigma'}{\sigma} \times 100\%$$

where σ and σ' represent tensile stress of pristine and healed hydrogels, respectively. The tests were conducted in triplicate for each specimen and expressed the results as mean ± standard deviation (SD).

SEM and EDX analyses

The surface morphology of PAA/PPy–Fe composite hydrogels was investigated with a JEOL (JSM-6500F, Tokyo, Japan) FE-SEM at an accelerating voltage of 10 kV. Previous to the scanning process, the samples were coated by a thin layer of platinum through the sputtering process. At the same time, energy dispersive X-ray (EDX) spectroscopy was performed to identify the elemental composition of hydrogels.

Antibacterial activity

Antibacterial activity of hydrogels was investigated *via* a disk diffusion method using *Escherichia coli* as Gram-negative bacteria with a final OD_{600} = 0.05 which were cultivated on overnight Luria-Bertani (LB) culture plate at 37 °C. The samples were adhered on the top of bacteria-suspended LB plate and kept with face-down position at 37 °C. Then, the antibacterial activity of samples was determined by measuring the inhibition zone of the samples after incubated for 8 and 12 h.

Electrical properties

The electrical properties of PAA/PPy–Fe hydrogels were characterized by using a conventional four-point probe technique to measured sheet resistance, using a set of Napson RT-7 and RG-7. PAA/PPy–Fe films were deposited on a glass slide and the thickness of the films was analyzed by surface profiler (Veeco Dektak 150 Stylus Profilometer). However, prior to the measurement, the water content in the hydrogels was maintained at 50% in order to eliminate the possibility of water in affecting the conductivity of hydrogels. The measurements were conducted in triplicate and expressed the results as mean ± standard deviation (SD). Moreover, the resistivity was calculated from resistance and film thickness, while conductivity (σ) of the sample was calculated using the following equation:

$$R = \frac{1}{R \times t}$$

where R denotes as sheet resistance and t represent the thickness of the film. Moreover, the resistant changes as a function of the strain of PAA/PPy–Fe composite hydrogels were measured using an oscilloscope (Tektronix DPO2012B).

Electrical conductivity application

The electrical conductivity application of PAA/PPy–Fe hydrogels was evaluated through a simple electrical circuit consisting of a light-emitting diode (LED) which was powered by 3 V batteries and connected with PAA/PPy–Fe hydrogels as illustrated in Fig. 1. To show the reversible restorability of PAA/PPy–Fe hydrogels, the hydrogel was cut-off and allowed to heal. Finally, the healed hydrogel was reconnected into the electrical circuit. The demonstration of PAA/PPy–Fe in conducting electricity in the circuit as indicated by the light on/off of LED.

Results and discussion

Preparation of PAA/PPy–Fe hydrogels

In this study, PAA/PPy–Fe composite hydrogels with fixed Fe content (0.5 mol% of AA) and variation of pyrrole concentration (0–20 mM) were fabricated. On the other hand, the hydrogels by varying Fe concentration (0.1–1 mol% of AA) and a fixed amount of pyrrole (15 mM) were synthesized. Firstly, the polymerization of AA and pyrrole was initiated by APS through free-radical polymerization (FRP). Prior to the polymerization, the mixture solution was degassed by using N_2 in order to remove O_2 contained in the solution, which can scavenge the radical during polymerization.[19] Further, the composite hydrogels were obtained by cross-linking (ionic interaction) between COO^- from PAA and Fe^{3+} from $FeCl_3$. The cross-linked hydrogels are able to heal autonomously after being damaged as shown in Fig. 2 which is ascribed to that ionic interaction. Moreover, the healed hydrogel could withstand stretching (Fig. 2b(iii)). Additionally, the self-healing processes observed by SEM displayed that both of the interfaces of the cut-off hydrogel adhered to each other. Such autonomous self-healing occurred in 3 h at 37 °C and showed no significant difference after healed for 12 h as shown in Fig. 1S.† Moreover, the hydrogels also possessed antimicrobial properties and conductive properties due to polypyrrole in the hydrogels.

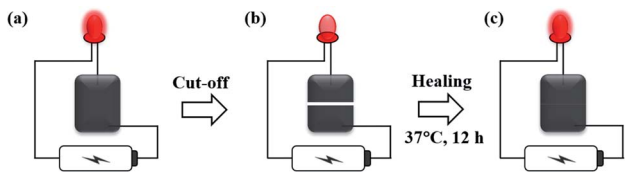

Fig. 1 Schematic illustration of an electrical circuit consisted of LED, powered by the battery and connected through (a) initial; (b) cut-off; and (c) healed PAA/PPy–Fe hydrogel.

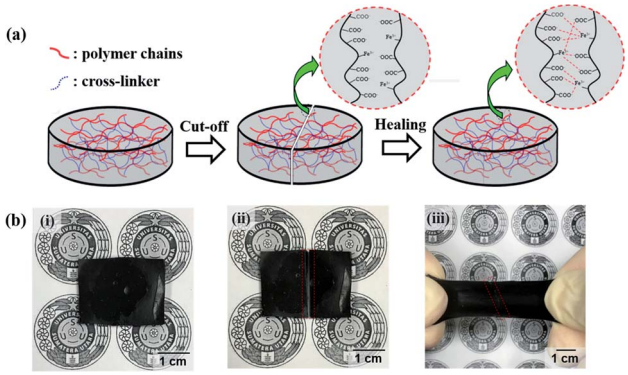

Fig. 2 (a) Illustration of self-healing processes of PAA/PPy–Fe hydrogels *via* ionic interaction and (b) photographs of PAA/PPy–Fe hydrogels in the condition of: (i) initial; (ii) cut-off; and (iii) healed hydrogel under stretching.

Chemical functionalities by FTIR analysis

The spectra of chemical functionalities of hydrogels are presented in Fig. 3. The peak at wavenumber 1650 cm^{-1} appeared

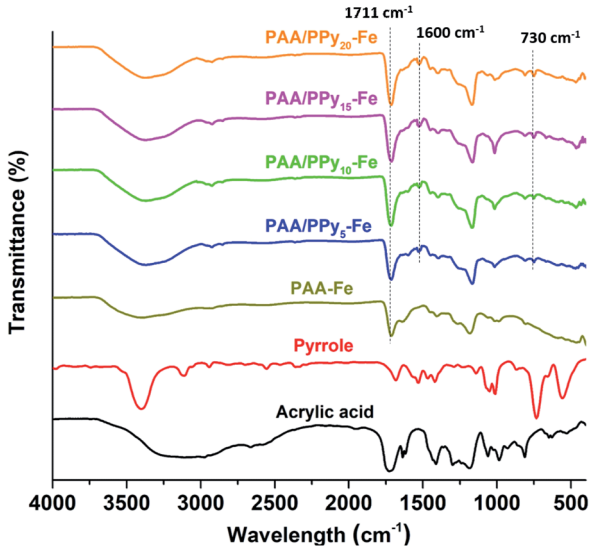

Fig. 3 FTIR spectra of acrylic acid, pyrrole and hydrogels with a variation of pyrrole concentration.

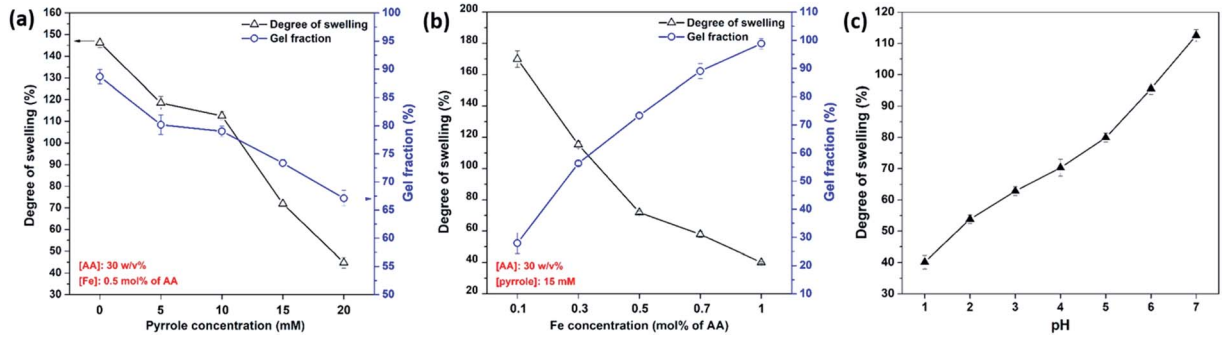

Fig. 4 Degree of swelling and gel fraction of hydrogels with (a) variation of pyrrole concentration; (b) variation of Fe concentration; and (c) the effect of pH on the swelling degree of PAA/PPy–Fe hydrogel.

in the spectra of acrylic acid corresponds to the C=C stretching vibration. In the spectra of hydrogels, the peak of C=C decreased significantly compared to the spectra of AA, which assigned to the polymerization of AA. The shifting peak from 1720 cm^{-1} (C=O) in AA spectrum to 1711 cm^{-1} in hydrogels spectra was assigned to the ionic interaction between carboxylic groups (COO–) from PAA and Fe^{3+}. As for the spectra of PAA/PPy–Fe composite hydrogels, the peaks at 1600 and 730 cm^{-1} were attributed to the bending vibrations of N–H and C–H of N-substituted of PPy, respectively. Furthermore, the stretching vibration of N–H from PPy is found in the range of 3400–3500 cm^{-1} which is overlapped with OH stretching vibration. However, by varying concentration of pyrrole, the spectra of

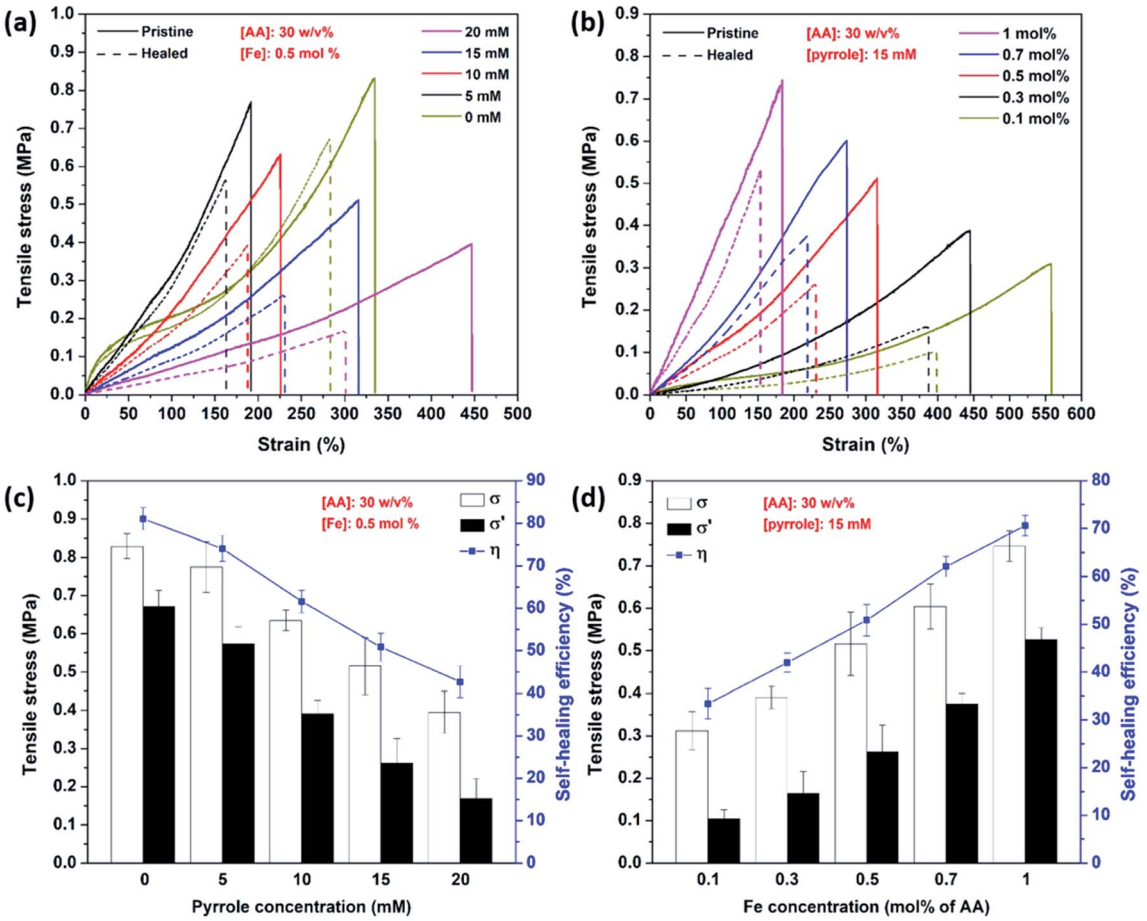

Fig. 5 Mechanical properties of tensile stress–strain curves of hydrogels with (a) variation of pyrrole concentration; and (b) variation of Fe concentration. Tensile stress-self-healing efficiency graphs of hydrogels with (c) variation of pyrrole concentration; and (d) variation of Fe concentration.

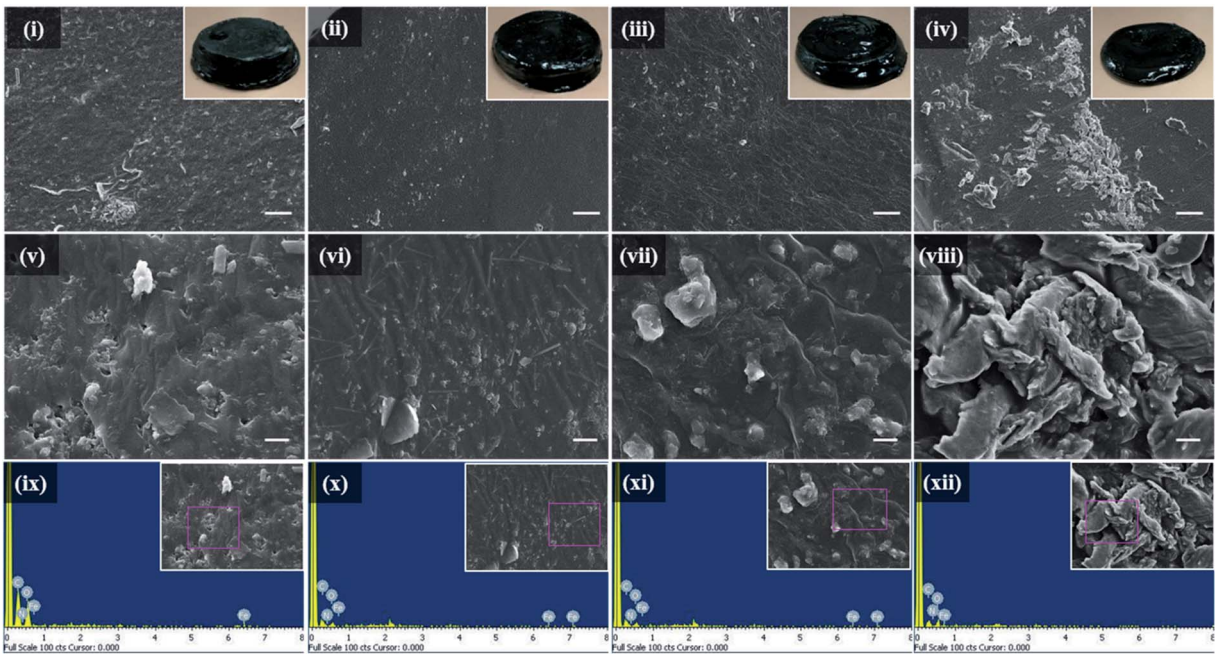

Fig. 6 SEM images of freeze-dried hydrogels: (i) PAA/PPy_5–Fe; (ii) PAA/PPy_{10}–Fe; (iii) PAA/PPy_{15}–Fe; and (iv) PAA/PPy_{20}–Fe hydrogels at magnification of ×500, (v–viii) at ×5000 and the EDX spectrum of hydrogels (ix–xii). Scale bars are (i–iv) 20 μm and (v–viii) 2 μm.

Table 1 The elementals composition by EDX analysis of PAA/PPy–Fe composite hydrogels

	Elements (atomic%)				
Hydrogels	C	N	O	Fe	Total (%)
PAA/PPy_5–Fe	55.86	1.01	41.98	1.15	100
PAA/PPy_{10}–Fe	47.09	9.32	40.77	2.82	
PAA/PPy_{15}–Fe	40.92	19.31	39.18	0.58	
PAA/PPy_{20}–Fe	40.49	20.67	38.01	0.83	

PAA/PPy–Fe hydrogels indicated insignificant alteration of the functional groups.

Equilibrium degree of swelling and gel fraction

The equilibrium degree of swelling and gel fraction of PAA/PPy–Fe hydrogels were shown in Fig. 4a. The results of swelling degree were 146.2, 118.5, 112.5, 71.9, and 44.8% for PAA–Fe, PAA/PPy_5–Fe, PAA/PPy_{10}–Fe, PAA/PPy_{15}–Fe, and PAA/PPy_{20}–Fe, respectively. The gel fraction decreased gradually from 88.7% to 67.1% with increasing concentration of pyrrole from 0 mM to 20 mM. The degrading values of gel fraction with increasing pyrrole concentration were ascribed to that pyrrole monomers react with $FeCl_3$ through oxidative polymerization[20] and resulted in less ionic interaction between COO^- from AA and Fe^{3+} from $FeCl_3$. Likewise, in the variation of Fe concentration, the swelling ratio showed a declining value from 169.9 to 40.1% as increase Fe concentration. On the contrary, the gel fraction of the prepared hydrogels increased from 27.9 to 98.8% with increasing Fe concentration. In this regards, such low gel fraction hydrogels contained less cross-linking junctions and less dense network, thus are able to expand more and absorb more water. Therefore, low gel fraction resulted in a high degree of swelling of the hydrogels. On the other hand, the swelling behaviour of PAA/PPy–Fe composite hydrogels was investigated in the pH range of 1–7 and represented in Fig. 4b. In this experiment, PAA/PPy_{10}–Fe was used as a representative to study the swelling behavior at different pH. Moreover, the ability of the hydrogel in retaining water increased gradually with increasing pH (1–7) of the swelling solution, which is ranged from 40.1% to 112.5%. The reason of such increasing trend at higher pH is due to the deprotonation of COOH groups in PAA ($pK_a = 4.2$) which cause the electrostatic repulsion and enlarge the networks in the hydrogel.[21,22]

Mechanical properties and self-healing efficiency

The tensile stress of PAA–Fe reached 0.83 MPa and with the addition of pyrrole with the concentration of 5, 10, 15, and 20 mM, the tensile stress was found to be 0.77, 0.64, 0.52, and 0.39 MPa, respectively. These results proved that the increase in pyrrole concentration could weaken the tensile stress of PAA/PPy–Fe composite hydrogels as can be seen in Fig. 5a. The result of gel fraction echoed such trend of tensile stress in which with the decrease of the cross-link density, the tensile stress will decrease.[23] Despite that, the PAA/PPy–Fe composite hydrogels show improvement in tensile strain from 180% to 448% with increasing pyrrole concentration from 5 to 20 mM. Subsequently, the self-healing efficiency of PAA/PPy–Fe composite hydrogels was evaluated by comparing the tensile stress of pristine and healed hydrogels. Herein, the fractured hydrogels were healed at 37 °C for 12 h prior to the tensile tests. The tensile test results of healed hydrogels (σ') displayed

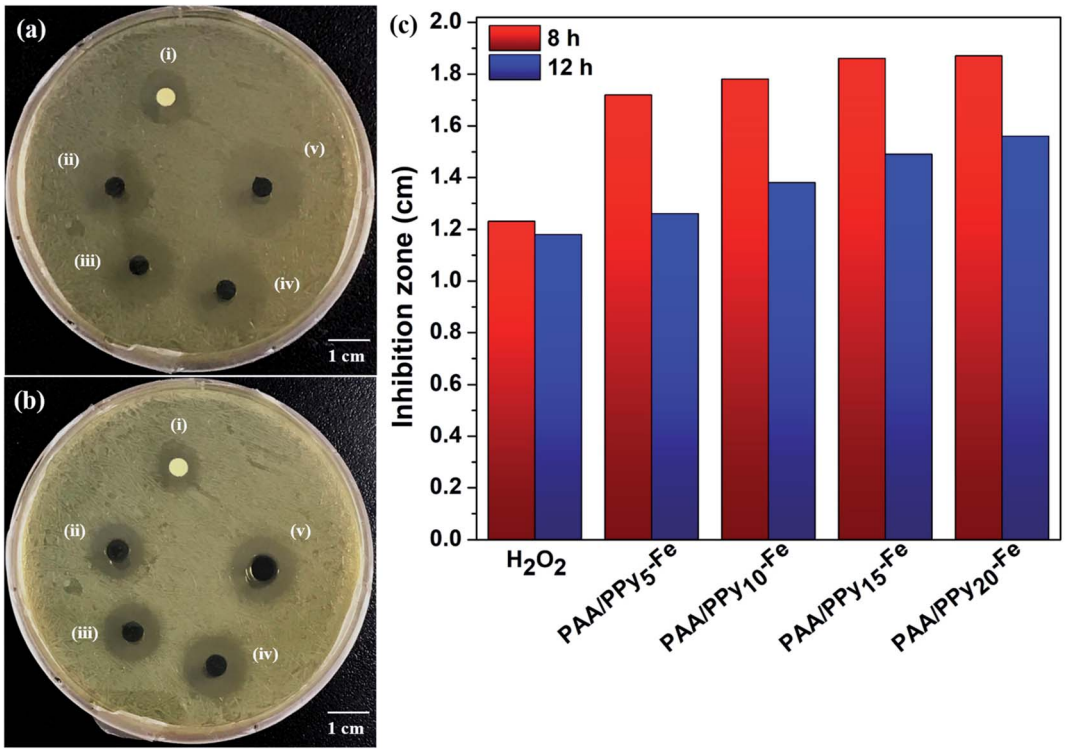

Fig. 7 Antibacterial activity of hydrogels: (i) H_2O_2; (ii) PAA/PPy_5–Fe; (iii) PAA/PPy_{10}–Fe; (iv) PAA/PPy_{15}–Fe; and (v) PAA/PPy_{20}–Fe on *E. coli* bacteria incubated at 37 °C for: (a) 8 h; (b) 12 h and (c) zone of inhibition of PAA/PPy–Fe hydrogels with different composition.

a decreasing trend from 0.57 MPa to 0.17 MPa with increasing pyrrole concentration from 5 mM to 20 mM. Hence, the self-healing efficiency (η) was calculated to be 74.1%, 61.6%, 50.8%, and 42.69% for PAA/PPy_5–Fe, PAA/PPy_{10}–Fe, PAA/PPy_{15}–Fe, and PAA/PPy_{20}–Fe, respectively (Fig. 5c). On the other hand, by increasing Fe concentration (0.1–1 mol% of AA), tougher hydrogels were produced in which the tensile stress increased from 0.31–0.74 MPa. As indicated by the result of tensile strain, the resulted hydrogels got more rigid and brittle with increasing Fe concentration. However, in agreement with the result of tensile stress, the self-healing efficiency of hydrogels exhibited a better result with increasing Fe concentration which raised from 33.37% to 70.58% (Fig. 5d). The decreasing in self-healing efficiency (η) might be correlated to the gel fraction of hydrogels, in which there might be less ionic interaction (–COO–Fe^{3+}) between the interface of two separated halves at lower gel fraction, therefore decrease the self-healing efficiency (η). Likewise, the results of both self-healing efficiency and gel fraction indicated a similar trend.

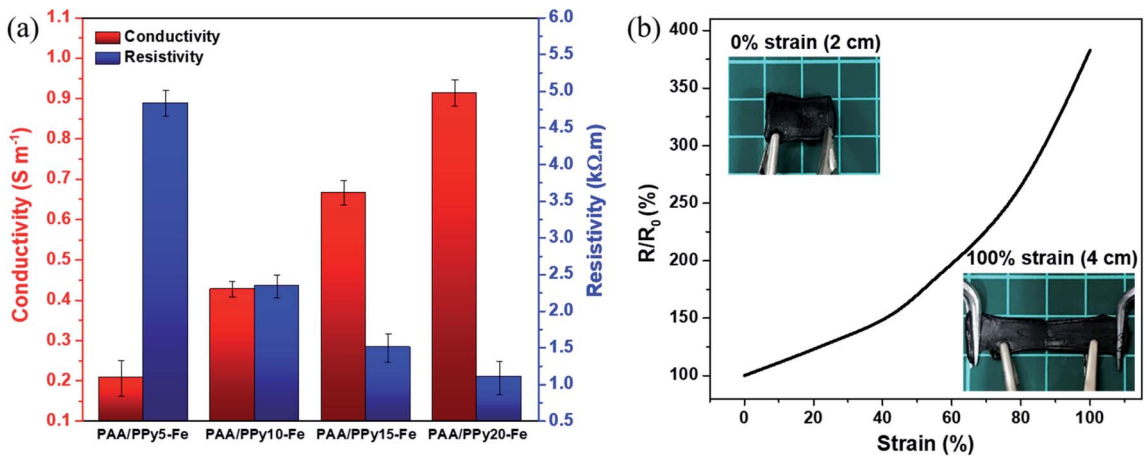

Fig. 8 (a) The electroconductivity and resistivity of PAA/PPy–Fe hydrogels with various concentration of pyrrole and (b) resistance ratio–strain curve of PAA/PPy_{20}–Fe hydrogel (the inserted photos are the strain at 0 and 100%).

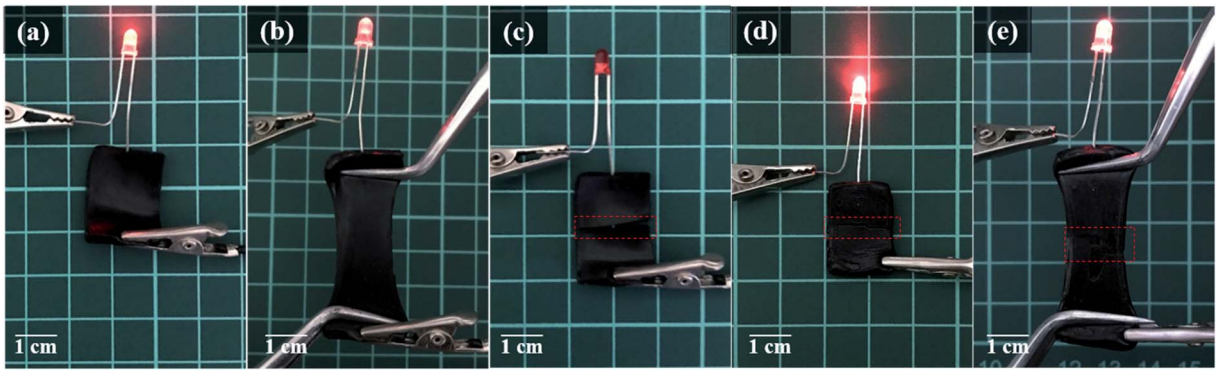

Fig. 9 Photographs of PAA/PPy–Fe hydrogel conducting electricity in an electrical circuit, (a) original; (b) stretched; (c) cut-off; (d) healed; and (e) healed and stretched hydrogel.

Surface morphology of hydrogels

The surface morphology of PAA/PPy–Fe composite hydrogels was observed using SEM and the images are depicted in Fig. 6(i–viii). As can be seen in the figure, all hydrogels exhibited a relative smooth surface. However, as pyrrole concentration increases, there are more particles can be observed on the surface of hydrogels which probably arises from polypyrrole. On the other hand, EDX analysis was performed to determine the elemental composition of PAA/PPy–Fe composite hydrogels. The EDX spectra of the hydrogels are presented in Fig. 6(ix–xii) and their elemental composition are summarized in Table 1. The results of EDX analysis revealed the presence of polypyrrole in the hydrogels indicated by N element and the atomic% of N increased with increasing of the pyrrole concentration.

Antibacterial activity

The antibacterial activity of PAA/PPy–Fe composite hydrogels was investigated toward *Escherichia coli* with a final OD_{600} value = 0.05. In this experiment, 10 μL of H_2O_2 on filter paper was used as the control group and all of the samples were cut with a size of 4 mm (Fig. 7a and b). The results revealed that the average diameter of inhibition zone incubated for 8 h increased slightly from 1.72 cm to 1.78, 1.86, and 1.87 cm for PAA/PPy_5–Fe, PAA/PPy_{10}–Fe, PAA/PPy_{15}–Fe, and PAA/PPy_{20}–Fe hydrogels, respectively (Fig. 7c). However, at longer incubation time of 12 h, the bactericidal abilities of composite hydrogels decreased and were found in the range of 1.26–1.56 cm. In this regard, both ferric ions (Fe^{3+}) and polypyrrole played an important role for the antibacterial properties in which the antibacterial mechanism of Fe^{3+} is the adsorption of Fe^{3+} on the bacteria and subsequently reduced to ferrous ions (Fe^{2+}).[24,25] Meanwhile, the positively charged polypyrrole seems to be responsible for the antibacterial activity by interacting with the bacterial cell wall and resulted in the death of bacteria.[26,27]

Electrical properties

The electrical properties (resistivity and conductivity) of PAA/PPy–Fe composite hydrogels were measured by the four-point probe method. Fig. 8a revealed that the resistivity of hydrogels decreased from 4.84 kΩ to 1.09 kΩ with increasing pyrrole concentration from 5–20 mM and at the same time, the electroconductivity increased from 0.21 S m^{-1} to 0.92 S m^{-1}. The increase in pyrrole concentration indicated an increase in conductivity as well and showed a good agreement with the results reported by Gan, *et al.* (2018) and Ren, *et al.* (2019).[28,29] Likewise, at higher cross-linking density, the rigid network was obtained and lead to hindrance for ions migration in the hydrogel networks therefore increase the resistance.[30] In addition, the resistance changes of composite hydrogel under strain were investigated and PAA/PPy_{20}–Fe hydrogel was used because it possesses the highest conductivity to compare to the other. Briefly, the resistance of PAA/PPy_{20}–Fe hydrogel increased with the increasing strain which was found to be 380% when the gel was stretched to 100% as can be seen in Fig. 8b. In this case, Fe^{3+} serves as dopant (oxidant) and Cl^- as a counter ion to be incorporated into the p-doped polypyrrole ring, in which the conductive properties arise from the oxidized form of polypyrrole–Cl.[31]

Electrical conductivity applications

The application of PAA/PPy–Fe composite hydrogels was evaluated by constructing a simple electrical circuit consisted of PAA/PPy_{15}–Fe connected with a light-emitting diode (LED) which was powered by 3 V batteries. PAA/PPy_{15}–Fe hydrogel was used by considering its self-healing efficiency and conductivity. After the electric was given, LED in the circuit was lighted-up which indicated the ability of PAA/PPy_{15}–Fe hydrogels to conduct electricity from the battery to LED as can be seen in Fig. 9a and b (stretched). In order to evaluate the reversible restorability, the hydrogel was cut into two-separated halves and the circuit was disconnected indicated by light-off as depicted in Fig. 9c. Then, the two broken pieces were allowed to heal at 70 °C for 2 h and reconstructed into the circuit. The result for after healed hydrogel proved that the LED can be lighted up again as shown in Fig. 9d and e (stretched). Nevertheless, as a result of resistance changes of PAA/PPy–Fe hydrogels under strain, the light intensity of LEDs was decreased (dim) when connected to both stretched pristine and healed hydrogels which can be seen visually in Fig. 9b and e.

Conclusion

In conclusion, self-healable PAA/PPy–Fe composite hydrogels with antimicrobial and conductive properties have been fabricated *via* free-radical polymerization in single-step preparation. The PAA/PPy–Fe composite hydrogels possess satisfying self-healing efficiency, bactericidal abilities and high in conductivity. The formation of PAA/PPy–Fe composite hydrogels is confirmed by the analyses of FTIR, SEM, and EDX. Furthermore, gel fraction (cross-linking density) of PAA/PPy–Fe composite hydrogels also plays a crucial role in the swelling, mechanical, and electrical properties of the resultant hydrogels. In addition, all the PAA/PPy–Fe composite hydrogels have been tested for their antibacterial activity on *Escherichia coli* and the result demonstrates that with higher pyrrole concentration, PAA/PPy–Fe composite hydrogels possess higher bactericidal effects. On the other hand, due to the conductive properties of PAA/PPy–Fe hydrogels, the hydrogel conducts electricity by lighting up the LED in an electrical circuit. Interestingly, the hydrogel demonstrates reversible restorability which is indicated by the healed hydrogel consistently conducts the electricity and lights up the LED.

Conflicts of interest

There are no conflicts to declare.

Acknowledgements

The authors would thank Universitas Sumatera Utara (USU) for the facilities to conduct the research.

Notes and references

1 Y. H. Tsou, J. Khoneisser, P. C. Huang and X. Xu, *Bioact. Mater.*, 2016, **1**, 39–55.
2 Z. Wei, J. He, T. Liang, H. Oh, J. Athas, Z. Tong, C. Wang and Z. Nie, *Polym. Chem.*, 2013, **4**, 4601.
3 W. Wang, R. Narain and H. Zeng, *Front. chem.*, 2018, **6**, 497.
4 H. R. Culver, J. R. Clegg and N. A. Peppas, *Acc. Chem. Res.*, 2017, **50**, 170–178.
5 A. S. Hoffman, *Adv. Drug Delivery Rev.*, 2012, **64**, 18–23.
6 N. A. Peppas, J. Z. Hilt, A. Khademhosseini and R. Langer, *Adv. Mater.*, 2006, **18**, 1345–1360.
7 S. Sun, L. B. Mao, Z. Lei, S. H. Yu and H. Colfen, *Angew. Chem., Int. Ed.*, 2016, **55**, 11765–11769.
8 M. Zhong, Y. T. Liu, X. Y. Liu, F. K. Shi, L. Q. Zhang, M. F. Zhu and X. M. Xie, *Soft Matter*, 2016, **12**, 5420–5428.
9 J. Pan, Y. Jin, S. Lai, L. Shi, W. Fan and Y. Shen, *Chem. Eng. J.*, 2019, **370**, 1228–1238.
10 H. Wang, G. Zha, H. Du, L. Gao, X. Li, Z. Shen and W. Zhu, *Polym. Chem.*, 2014, **5**, 6489–6494.
11 D. Gan, T. Xu, W. Xing, X. Ge, L. Fang, K. Wang, F. Ren and X. Lu, *Adv. Funct. Mater.*, 2019, **29**, 1–11.
12 J. H. Min, M. Patel and W. G. Koh, *Polymers*, 2018, **10**, 1–36.
13 G. Kaur, R. Adhikari, P. Cass, M. Bown and P. Gunatillake, *RSC Adv.*, 2015, **5**, 37553–37567.
14 D. L. Wise, G. E. Wnek, D. J. Trantolo, T. M. Cooper, J. D. Gresser and D. Marcel, *Electrical and Optical Polymer Systems: Fundamentals, Methods, and Application*, Marcel Dekker, New York, 1998.
15 R. K. Pal, S. Pradhan, L. Narayanan and V. K. Yadavalli, *Sens. Actuators, B*, 2018, **259**, 498–504.
16 A. Simaite, F. Mesnilgrente, B. Tondu, P. Souères and C. Bergaud, *Sens. Actuators, B*, 2016, **229**, 425–433.
17 D. Uppalapati, B. J. Boyd, S. Garg, J. Travas-Sejdic and D. Svirskis, *Biomaterials*, 2016, **111**, 149–162.
18 V. Khomenko, E. Frackowiak, V. Barsukov and F. Beguin, *New Carbon Based Materials for Electrochemical Energy Storage Systems*, 2006, pp. 41–50.
19 V. A. Bhanu and K. Kishore, *Chem. Rev.*, 1991, **91**, 99–117.
20 Y. Lu, W. He, T. Cao, H. Guo, Y. Zhang, Q. Li, Z. Shao, Y. Cui and X. Zhang, *Sci. Rep.*, 2014, **4**, 5792.
21 E. O. Akala, P. Kopeckova and J. Kopecek, *Biomaterials*, 1998, **19**, 1037–1047.
22 J. E. Elliott, M. Macdonald, J. Nie and C. N. Bowman, *Polymer*, 2004, **45**, 1503–1510.
23 B. Depalle, Z. Qin, S. J. Shefelbine and M. J. Buehler, *J. Mech. Behav. Biomed. Mater.*, 2015, **52**, 1–13.
24 R. Tian, X. Qiu, P. Yuan, K. Lei, L. Wang, Y. Bai, S. Liu and X. Chen, *ACS Appl. Mater. Interfaces*, 2018, **10**, 17018–17027.
25 H. Q. Sun, X. M. Lu and P. J. Gao, *Braz. J. Microbiol.*, 2011, **42**, 410–414.
26 A. Varesano, C. Vineis, A. Aluigi, F. Rombaldoni, C. Tonetti and G. Mazzuchetti, *Fibers Polym.*, 2013, **14**, 36–42.
27 W. Zhou, L. Lu, D. Chen, Z. Wang, J. Zhai, R. Wang, G. Tan, J. Mao, P. Yu and C. Ning, *J. Mater. Chem. A*, 2018, **6**, 3128–3135.
28 D. Gan, L. Han, M. Wang, W. Xing, T. Xu, H. Zhang, K. Wang, L. Fang and X. Lu, *ACS Appl. Mater. Interfaces*, 2018, **10**, 36218–36228.
29 K. Ren, Y. Cheng, C. Huang, R. Chen, Z. Wang and J. Wei, *J. Mater. Chem. B*, 2019, **7**, 5704–5712.
30 W. K. Shin, J. Cho, A. G. Kannan, Y. S. Lee and D. W. Kim, *Sci. Rep.*, 2016, **6**, 26332.
31 R. Buitrago-Sierra, M. J. García-Fernández, M. M. Pastor-Blas and A. Sepúlveda-Escribano, *Green Chem.*, 2013, **15**, 1981–1990.